

Graph-convolution neural network-based flexible docking utilizing coarse-grained distance matrix

Amr H. Mahmoud,^{†,‡} Jonas F. Lill,[‡] and Markus A. Lill^{*,‡}

[†]*Department of Medicinal Chemistry and Molecular Pharmacology, College of Pharmacy, Purdue University, 575 Stadium Mall Drive, West Lafayette, Indiana 47906, United States*

[‡]*Department of Pharmaceutical Sciences, University of Basel, Klingelbergstrasse 50, 4056 Basel, Switzerland*

E-mail: markus.lill@unibas.ch

Phone: ++41 61 2076135

Abstract

Prediction of protein-ligand complexes for flexible proteins remains still a challenging problem in computational structural biology and drug design. Here we present two novel deep neural network approaches with significant improvement in efficiency and accuracy of binding mode prediction on a large and diverse set of protein systems compared to standard docking. Whereas the first graph convolutional network is used for re-ranking poses the second approach aims to generate and rank poses independent of standard docking approaches. This novel approach relies on the prediction of distance matrices between ligand atoms and protein C_{α} atoms thus incorporating side-chain flexibility implicitly.

Introduction

Structure-based drug design is an essential tool and an important pillar in Computer-aided Drug Design (CADD) for efficient lead discovery and optimization. CADD methods such as docking aim to identify novel binders to a target protein and to predict the structure of protein-ligand complexes. Docking is still widely applied using a rigid protein as template in CADD projects, ignoring the representation of the different conformations that the binding-site can assume.

The importance of modelling protein flexibility in docking, however, has been recognized already in early docking studies. In 1999 Murray et al.¹ demonstrated the shortcomings of docking to rigid proteins by carrying out rigid cross docking for three enzymes (thrombin, thermolysin and the influenza virus neuroaminidase). Each ligand was docked to the protein structures of all complexes available for each enzyme. The authors found that in 51% of the cases the program failed to dock the small molecules directly and highlighted the importance of modeling protein flexibility in computational docking.¹ Later, Englebienne & Moitessier showed that the accuracy of many scoring functions can be deteriorated by protein flexibility and solvation.² A large number of reviews discuss the importance of incorporating protein flexibility in docking algorithms while focusing on side-chain, backbone and domain movements necessary for the protein to accommodate different ligands.³⁻⁷

Incorporating protein flexibility into molecular docking is a difficult optimization problem involving a large number of degrees of freedom that represent the receptor flexibility. Approaches to incorporate receptor flexibility range from the use of soft-core potentials, multiple protein structures (ensemble docking) or the active sampling of protein conformations during energy optimization of the ligand (induced-fit docking).^{8,9} Due to the computational complexity of the problem, for many practical uses, flexible docking is still a challenging task and full incorporation of protein flexibility is computationally not feasible. In summary, there is a significant demand for efficient algorithms to handle flexible proteins in docking.

Several limitations for improving flexible docking methodology exist. Most of the published

methods are optimized or benchmarked on limited data sets with a very limited set of targets.⁹ While this practice was acceptable in the past due to the limitation of computational resources, this is no longer the case nowadays. Validation has to be carried out using large test sets with a wide range of different targets. Only such a validation procedure allows to identify the shortcomings of current and newly developed algorithms. This is essential for systematic improvement of flexible protein docking methodologies.

Additionally, flexible docking is more resource and time intensive than rigid docking. The application of flexible docking to virtual screening of large libraries is still unrealistic. The number of degrees of freedom in flexible protein docking is significantly higher compared to rigid docking, leading to an increase in rate of false-positives and intensive usage of computational resources. Thus, there is a crucial need to develop new methods that rely on efficient algorithms and heuristics to lessen the computational requirements and allow an accurate widespread implementation of flexible docking engines.

In rigid docking applications deep-learning methods proved to be useful in achieving unprecedented accuracy in pose prediction.¹⁰⁻¹² In this work, we aim to utilize deep learning to improve the quality of flexible docking approaches. We will demonstrate that our deep learning-based concepts increase the accuracy of flexible docking with concurrent improvement in sampling efficiency. Two neural-network-based methods are presented here making initial steps towards this overarching aim (Figure 1). The first method, named re-ranking by gated attention neural network (RerankGAT) method, re-evaluates docking poses generated by standard docking approaches, while the second method, named pose generation by neural-network predicted distance matrix (PoseNetDiMa), is based on predicting and utilizing the distance matrix, which represents the relation between ligand and protein atoms, for pose generation and ranking.

Concepts using predictions of distance matrices have proven to be useful in many branches of bioinformatics and cheminformatics. AlphaFold, for example, enabled the an initio prediction of 3D-protein structures with a higher accuracy than any other state-of-the-art

methods.^{13,14} Another example used Wasserstein generative adversarial networks (GAN) to generate valid conformations of organic molecules.¹⁵ Our concept of using the prediction of distance matrices between proteins and ligands is the first in the domain of docking or protein-ligand interactions in general.

The RerankGAT method uses a graph representation for each possible ligand-protein pose and a distance-aware gated graph attention mechanism in order to learn to classify the ligand poses.¹⁶⁻¹⁸ Details are discussed in the following Materials and Methods section. It is important to emphasize that the RerankGAT methods in this work can boost the ranking of docking poses in case of docking success but cannot address sampling failure, i.e. failure to generate native-like poses independent of their subsequent ranking.

The PoseNetDiMa method predicts the distance matrix between the C_α atoms of the target protein and all heavy atoms of the ligand to be docked. C_α atoms were chosen to implicitly include side-chain flexibility without explicit sampling. The method uses coordinates of the C_α atoms and the ligand topology as input. A graph neural network with a global attention mechanism is trained to predict the pairwise distances between protein C_α and ligand heavy atoms.¹⁹⁻²² The model relies on the heterogeneous graph attention concept²³ where two different types of graphs are encoded (Figure 2): One graph represents the protein using the C_α atoms as nodes colored by the type of amino acid. Edges between nodes are defined based on the Euclidean distance between C_α atoms. The other graph encodes the ligand, where nodes and edges are represented by heavy atoms and covalent bonds. No spatial information is included in the ligand graph, as information about ligand conformation has to be predicted in the docking stage based on the predicted distance matrix. In our implementation both graphs are fused into one graph with extended feature vectors as described in subsequent sections.

The PoseNetDiMa method is far more versatile since the predicted distance matrix can be used in multiple ways: First, the predicted distance matrix can provide restraints necessary to confine the solutions within a limited space, thus enabling exploration of configurational space

in a reasonable time. Second, generated poses can be filtered according to their correlation with the predicted distance matrix. Third, direct reconstruction of the ligand within the binding pocket based on the distance matrix is possible. In summary, the predicted distance matrix can be used in machine-learning assisted docking or re-scoring of poses. Thus, in contrast to RerankGAT, PoseNetDiMa was designed to increase the number of systems for which native docking solutions are identified compared to standard flexible docking.

Materials and Methods

Training Data

The general set from PDBbind was used for training and initial validation of the models. To generate poses for model training and validation, flexible docking was performed using Smina.²⁴ Unbiased selection of flexible residues was chosen, where any residue was considered flexible if it is located within 4 Å of the ligand in the X-ray complex structure. The search volume was defined by the centroid of the co-crystallized ligand, adding a padding of 8 Å to the box encompassing the ligand. Exhaustiveness is set to 8 with 50 modes being requested and using 8 threads per docking job. For validation purposes, the data set was split into four groups and 4-fold cross-validation was performed.

Validation and Quality Assessment using Cross Docking

The quality of the models was further assessed using cross docking. The data sets used for this assessment comprises a large number of targets which vary among each other according to their difficulty in flexible docking. The total number of ligands which were docked were around 4500 ligands from 95 targets with an average of 45 ligands per target (Table 1). All ligands were docked with flexible side chains with the same settings used for docking the General Set from PDBBind (cf. Section Training Data). The dataset is consistent in coverage with the Disco dataset.²⁵ In contrast to the study of Wierbowski et al.²⁵ flexible docking on

one template protein structure was performed instead of rigid cross-docking.

Table 1: Targets and number of ligands used in cross-docking experiments.

	Target	PDB	Description	N°
1	THB	1Q4X	Thyroid hormone receptor beta-1	14
2	WEE1	3BIZ	Serine/threonine-protein kinase WEE1	8
3	KITH	2B8T	Thymidine kinase	2
4	ADRB1	2VT4	Beta-1 adrenergic receptor	15
5	HDAC2	3MAX	Histone deacetylase 2	3
6	ANDR	2AM9	Androgen Receptor	92
7	XIAP	3HL5	Inhibitor of apoptosis protein 3	21
8	MCR	2AA2	Mineralocorticoid receptor	18
9	PRGR	3KBA	Progesterone receptor	18
10	GCR	3BQD	Glucocorticoid receptor	17
11	ESR2	2FSZ	Estrogen receptor beta	32
12	FPPS	1ZW5	Farnesyl diphosphate synthase	30
13	FA10	3KL6	Coagulation factor X	104
14	HMDH	3CCW	HMG-CoA reductase	19
15	ADRB2	3NY8	Beta-2 adrenergic receptor	9
16	GLCM	2V3F	Beta-glucocerebrosidase	9
17	RXRA	1MV9	Retinoid X receptor alpha	42
18	PA2GA	1KVO	Phospholipase A2 group IIA	8
19	HIVRT	3LAN	Human immunodeficiency virus type 1 reverse transcriptase	169
20	ESR1	1SJ0	Estrogen receptor alpha	104
21	GRIA2	3KGC	Glutamate receptor ionotropic, AMPA 2	84
22	KIF11	3CJO	Kinesin-like protein 1	32

Table 1: Continued

23	FKB1A	1J4H	FK506-binding protein 1A	26
24	VGFR2	2P2I	Vascular endothelial growth factor receptor 2	24
25	THRB	1YPE	Thrombin	216
26	TRY1	2AYW	Trypsin I	169
27	RENI	3G6Z	Renin	46
28	PGH1	2OYU	Cyclooxygenase-1	19
29	TGFR1	3HMM	TGF-beta receptor type I	15
30	PPARA	2P54	Peroxisome proliferator-activated receptor al- pha	15
31	JAK2	3LPB	Tyrosine-protein kinase JAK2	48
32	AKT1	3CQW	Serine/threonine-protein kinase AKT	11
33	PDE5A	1UDT	Phosphodiesterase 5A	26
34	MAPK2	3M2W	MAP kinase-activated protein kinase 2	13
35	LKHA4	3CHP	Leukotriene A4 hydrolase	39
36	HS90A	1UYG	Heat shock protein HSP 90-alpha	175
37	CAH2	1BCD	Carbonic anhydrase II	242
38	BRAF	3D4Q	Serine/threonine-protein kinase B-raf	46
39	PNPH	3BGS	Purine nucleoside phosphorylase	6
40	NRAM	1B9V	Neuraminidase	12
41	KIT	3G0E	Stem cell growth factor receptor	6
42	HIVPR	1XL2	Human immunodeficiency virus type 1 pro- tease	394
43	UROK	1SQT	Urokinase-type plasminogen activator	14
44	HIVINT	3NF7	Human immunodeficiency virus type 1 inte- grase	8

Table 1: Continued

45	HXK4	3F9M	Hexokinase type IV	24
46	CDK2	1H00	Cyclin-dependent kinase 2	310
47	MK10	2ZDT	c-Jun N-terminal kinase 3	59
48	DEF	1LRU	Peptide deformylase	10
49	PGH2	3LN1	Cyclooxygenase-2	30
50	PPARD	2ZNP	Peroxisome proliferator-activated receptor delta	21
51	MMP13	830C	Matrix metalloproteinase 13	28
52	MK14	2QD9	MAP kinase p38 alpha	176
53	PTN1	2AZR	Protein-tyrosine phosphatase 1B	74
54	PUR2	1NJS	GAR transformylase	9
55	MK01	2OJG	MAP kinase ERK2	69
56	DPP4	2I78	Dipeptidyl peptidase IV	71
57	DYR	3NXO	Dihydrofolate reductase	11
58	ADA	2E1W	Adenosine deaminase	15
59	MET	3LQ8	Hepatocyte growth factor receptor	49
60	FAK1	3BZ3	Focal adhesion kinase 1	21
61	ROCK1	2ETR	Rho-associated protein kinase 1	12
62	ACE	3BKL	Angiotensin-converting enzyme	8
63	PLK1	2OWB	Serine/threonine-protein kinase PLK1	10
64	MP2K1	3EQH	Dual specificity mitogen-activated protein kinase kinase 1	8
65	ACES	1E66	Acetylcholinesterase	41
66	ITAL	2ICA	Leukocyte adhesion glycoprotein LFA-1 alpha	13
67	IGF1R	2OJ9	Insulin-like growth factor I receptor	13

Table 1: Continued

68	TRYB1	2ZEC	Tryptase beta-1	13
69	FA7	1W7X	Coagulation factor VII	42
70	ABL1	2HZI	Tyrosine-protein kinase ABL	39
71	GRIK1	1VSO	Glutamate receptor ionotropic kainate 1	23
72	ADA17	2OI0	ADAM17	12
73	BACE1	3L5D	Beta-secretase 1	262
74	SRC	3EL8	Tyrosine-protein kinase SRC	48
75	PARP1	3L3M	Poly [ADP-ribose] polymerase-1	17
76	LCK	2OF2	Tyrosine-protein kinase LCK	32
77	CSF1R	3KRJ	Macrophage colony stimulating factor receptor	12
78	CP2C9	1R9O	Cytochrome P450 2C9	3
79	ALDR	2HV5	Aldose reductase	3
80	SAHH	1LI4	Adenosylhomocysteinase	3
81	AOFB	1S3B	Monoamine oxidase B	3
82	PPARG	2GTK	Peroxisome proliferator-activated receptor gamma	116
83	FABP4	2NNQ	Fatty acid binding protein adipocyte	22
84	AKT2	3D0E	Serine/threonine-protein kinase AKT2	10
85	HDAC8	3F07	Histone deacetylase 8	7
86	EGFR	2RGP	Epidermal growth factor receptor erbB1	81
87	PYGM	1C8K	Muscle glycogen phosphorylase	18
88	CXCR4	3ODU	C-X-C chemokine receptor type 4	4
89	PYRD	1D3G	Dihydroorotate dehydrogenase	4
90	AMPC	1L2S	Beta-lactamase	59

Table 1: Continued

91	FNTA	3E37	Protein farnesyltransferase / geranylgeranyl-transferase type I alpha subunit	23
92	CASP3	2CNK	Caspase-3	21
93	TYSY	1SYN	Thymidylate synthase	11
94	AA2AR	3EML	Adenosine A2a receptor	2
95	CP3A4	3NXU	Cytochrome P450 3A4	7

Model Features

For both network models, basic chemical properties of atoms were used as initial node features. Those features include an atom’s elemental type, connectivity index, aromaticity, implicit valence, partial charge estimates, number of attached hydrogen atoms, surface area contributions (Labute ASA in rdkit and TPSA), Crippen LogP, Crippen MR and electrotopological State descriptors known as EState in rdkit. Bond featurization depends on the bond type, bond conjugation and whether the bond is a ring bond. In the PoseNetDiMa model, however, which relies on a coarse-grained representation of the protein, the nodes in the protein graph represent the C_α atoms of the amino acids of the binding site with one-hot-encoding for the twenty different amino acids. Features describing the physicochemical properties of each amino acid (i.e. polar, charged, hydrophobic, aromatic side chain) are added to the feature vector describing the nodes of the protein graph. To generate a single, heterogeneous graph containing both ligand and protein nodes, the ligand and protein node features are concatenated into one feature vector $F_i = (\mathbf{f}_i^{(L)}, \mathbf{f}_i^{(P)})$. Since C_α atoms are not covalently bonded, the edges were represented using virtual bonds that reflect pairwise distances between two nodes being within 7 Å. In detail, five distance bins between 2 Å and 7 Å are generated, and an edge between two C_α atoms within a maximum distance of 7 Å is colored by its association with the matching distance bin using one-hot encoding. For

example, an edge between two C_α atoms with distance of 5.7 Å will have the feature vector (0, 0, 0, 1, 0). To combine the heterogeneous bond features of ligand and protein, the feature vectors are concatenated: $F_{ij} = (\mathbf{f}_{ij}^{(L)}, \mathbf{f}_{ij}^{(P)})$.

Graph Neural Network Models

Pose re-ranking model: RerankGAT

The model for pose re-ranking utilizes the Graph Neural Network algorithm described by Lim et al.¹⁶ The network was gated with an attention mechanism that takes distances into consideration.

Model for prediction of distance matrix: PoseNetDiMa

The PoseNetDiMa model is inspired by the work of Jin et al.^{21,22} on synthesis prediction. In our work, a similar network as in Jin et al.^{21,22} is used with the main aim to predict protein-ligand distance matrices that could be used as distance restraints during pose sampling or for pose filtering and re-scoring. The network tries to identify the correspondence between each atom of the ligand and C_α atoms comprising the protein-binding site .

In a first step, the nodes of both protein and ligand graph are encoded using a graph neural network (Figure 4 A). To encode the hidden features $\mathbf{h}_v^{(l)}$ of a node v in layer l , messages \mathbf{m}_{uv} from neighboring nodes $u \in N(v)$ are collected. To compute the message between u and v , the current node feature $\mathbf{h}_u^{(l-1)}$ and edge feature \mathbf{F}_{uv} are concatenated and used as input of a neural network (Figure 4 A) with ReLU activation function τ :

$$\mathbf{m}_{vu} = \tau(\mathbf{V}[\mathbf{h}_u^{(l-1)}, \mathbf{F}_{uv}]) \tag{1}$$

After collecting all message from neighboring nodes, the previous hidden feature $\mathbf{h}_v^{(l-1)}$ of node v is added in a skip connection and a subsequent neural network finally encodes new hidden features

$$\mathbf{h}_v^{(l)} = \tau(\mathbf{U}_1 \mathbf{h}_v^{(l-1)} + \mathbf{U}_2 \sum_{u \in N(v)} \tau(\mathbf{V}[\mathbf{h}_u^{(l-1)}, \mathbf{F}_{uv}])) \quad (2)$$

where $\mathbf{h}_v^{(0)} = \mathbf{F}_v$ and $\mathbf{U}_1, \mathbf{U}_2, \mathbf{V}$ are shared weights.

After L steps of graph convolutions, the current hidden feature vector $\mathbf{h}_v^{(l)}$ is transformed into a final local feature vector \mathbf{c}_v (Figure 4 B). First, $\mathbf{h}_v^{(l)}$, neighboring feature vectors $\mathbf{h}_u^{(l)}$ and corresponding edges undergo additional tensor multiplications by $\mathbf{W}^{(0)}$, $\mathbf{W}^{(1)}$ and $\mathbf{W}^{(2)}$. Subsequent Hadamard products between the three resulting entities generates the final local feature vector \mathbf{c}_v :

$$\mathbf{c}_v = \mathbf{W}^{(2)} \mathbf{h}_v^{(L)} \odot \sum_{u \in N(v)} \mathbf{W}^{(0)} \mathbf{h}_u^{(L)} \odot \mathbf{W}^{(1)} \mathbf{F}_{uv} \quad (3)$$

\mathbf{c}_v is a feature vector that locally encodes the chemical environment of the atom.

To predict the likely distance between ligand atoms and protein C_α atoms, the currently distinct ligand and protein graphs need to be connected. In other words, information needs to be shared between both graphs. The main idea is that the interaction strengths between different residue types and ligand atom types varies (e.g. hydrogen bonds differ in distance dependency and strength compared to hydrophobic contacts). Whereas the local environment of a node within one of the graph is captured according to each atom’s connectivity with its neighbors, the global environment, i.e. protein-ligand interactions, is incorporated through a global attention mechanism which allows for weighted information exchange between nodes of the two different graphs (Figure 4 C). The attention score α_{uv} between nodes u and v is derived by

$$\alpha_{uv} = \sigma(\mathbf{u}^T \tau(\mathbf{P}_a \mathbf{c}_u + \mathbf{P}_a \mathbf{c}_v + \mathbf{P}_b \mathbf{b}_{uv})) \quad (4)$$

where $\sigma(\cdot)$ is the sigmoid function, and \mathbf{b}_{uv} is a feature vector that represents information about the relationship between u and v , i.e. whether the two nodes represent protein-protein,

ligand-protein or ligand-ligand pairwise interactions or covalent bonds.

The global feature representation g_u of node u is then calculated as the weighted sum of all other surrounding nodes where the weights correspond to the attention factors (Figure 4 D):

$$\mathbf{g}_u = \sum_v \alpha_{uv} \mathbf{c}_v \tag{5}$$

Finally, the distance between two nodes u and v , e.g. ligand atom u and protein C_α atom v is computed (Figure 4 E) by

$$d_{uv} = \mathbf{u}^T \tau(\mathbf{M}_a \mathbf{g}_u + \mathbf{M}_a \mathbf{g}_v + \mathbf{M}_b \mathbf{f}_{uv} + \mathbf{P}_a \mathbf{c}_u + \mathbf{P}_a \mathbf{c}_v) \tag{6}$$

Training. The network is finally trained to reproduce the experimentally measured distances y_{uv} between ligand atoms u and protein C_α atoms v . The in-dependant prediction of each label is performed due to the quadratic complexity of the problem. The interaction labels can be determined by the product of N ligand atoms and M C_α atoms and this quadratic complexity prevents higher-order predictions.

Docking using PoseNetDiMa

Similar to RerankGAT, PoseNetDiMa can be used for re-ranking poses obtained from standard flexible docking such as Smina. As Smina is unable to generate native-like poses for a large number of targets, we tested if the predicted distance matrices could be directly used for both posing and ranking phases in docking. A scheme of the overall docking scheme based on PostNetDiMa is shown in Figure 5.

First, the distance matrix for the protein-ligand system of interest is predicted using PostNetDiMa. For every ligand atom, all possible locations are computed based on the predicted distance matrix using all possible triplets of C_α atoms in the binding site. Those points are clustered using Quality Threshold (QT) clustering algorithm with a radius of 1

Å. Clustering is stopped either when half of all possible points are assigned to cluster or a maximum number of three clusters is identified for an atom. Pharmacophore models are generated from the clusters with one element per atom. For each atom the used cluster center is selected randomly, generating a maximum number of 25 pharmacophores. Docking is performed to the pharmacophore models using LSAAlign.²⁶ Those poses are rescored using iDock on atomic density maps. Those density maps are 3D grids where the density of a ligand atom i at grid point k is obtained from the product of normal distribution functions centered around the predicted distance d_{ji} between ligand atom i and C_α atom j

$$p_k^i = \prod_j \exp(-0.5 \cdot (r_{jk} - d_{ji})^2) \quad (7)$$

where r_{jk} is the distance between protein atoms j and grid point k .

Results

General Set Evaluation

Four-fold cross validation was carried out using the General-set from PDBbind. The cumulative results of only the test sets in the four cross-validation runs are reported. First, we tested the re-ranking performance of RerankGAT based on the poses obtained from Smina docking. Smina was only able to generate native-like poses (RMSD < 2 Å to native pose) for 66 % of all systems (Figure 6, top). For those systems with native-like poses, Smina ranks 59 % of them as top-1 and 87 % within the top-5 poses (Figure 6, bottom).

Figure 6 shows that the RerankGAT deep-learning model could considerably boost the ranking of pose-prediction in case a native-like pose was sampled by Smina. For almost all systems, for which a native-like pose was sampled, that pose was retrieved within the top-5 re-ranked poses. For 78 % of systems with native-like pose, that pose was ranked at top-1 position.

In response to the high number of systems, for which no native-like pose could be generated using Smina, PoseNetDiMa was designed to generate poses based on the predicted distance matrix between protein residues and ligand atoms. First, we investigated the quality of PoseNetDiMa to predict experimental distance matrices. Figure 7 (top) shows that for the majority of systems a correlation with $r^2 > 0.5$ could be achieved, for half of the systems a correlation even larger than 0.8. Interestingly, there is a correlation between number of systems with native-like poses and quality in distance matrix prediction (Figure 7, bottom). For example, 80 % of systems with high distance-matrix quality ($r^2 > 0.8$) have near-native poses, while only 50 % with poor distance matrix quality ($r^2 < 0.5$). Initial analysis indicates that the distance matrix for systems with high flexibility and particular solvent-exposure, that may have alternative binding poses, are difficult to predict. Those systems also show no robust prediction in binding poses in docking.²⁷

Cross-Docking Assessment

For additional validation, the same analysis was performed on cross docking on 95 targets with different levels of difficulty. Some targets are known to have high failure rate in cross docking such as Cytochrome P450 3A4 and Caspase-3. Smina was used for flexible docking of the cross-docking dataset and the poses were re-scored using the graph-attention neural network model trained on the general set of PDBbind (Figure 8). The first observation is that there are a higher number of systems with native-like poses compared to the general set of PDBbind (81 % versus 66 %). The reason for this difference is that for each target system, the protein structure with the highest success rate was selected for cross-docking studies following a previous protocol.²⁵

The higher number of systems with native-like poses resulted in higher number of native-like poses identified in the top-5 ranked list with rescoreGAT (77 %) again outperforming Smina scoring (64 %). In contrast, the performance for identifying a native-like pose in the top-1 position remained unchanged in the cross-docking study compared to flexible docking

to PDBbind.

Figure 9 shows similar accuracy in predicting the distance matrix for the cross-docking dataset compared to the PDBbind dataset, and the same trend of overall better prediction of the distance matrix for systems with more likely success in generating native-like poses.

Re-ranking of poses using PoseNetDiMa

Next, we explored the potential of PoseNetDiMa to re-rank poses obtained from Smina. Whereas the similarity between native and docked pose is typically measured by their RMSD value, alternatively the similarity of their corresponding protein-ligand distance matrices could be used (Figure 10). Thus, assuming the distance matrix predicted by PoseNetDiMa is similar to the experimentally known distance matrix, the docked poses could be translated into distance matrices and ranked by their similarity to the predicted distance matrix. Based on this idea, the hypothesis has been that pose ranking could be improved using the predicted distance matrix from PoseNetDiMa.

The analysis was performed on those systems for which the docking engine was able to generate near-native poses. As shown in Figure 11 (left), PoseNetDiMa significantly improves pose ranking, even outperforming RerankGAT by a significant margin. Whereas, Smina is only able to rank 47 % of systems with native-like poses as top-1, PoseNetDiMa increases this percentage to 82 %. Adding native poses to the pool of docked poses further increases this percentage to 89 %.

Docking using PoseNetDiMa

Docking using PoseNetDiMa was performed on the cross-docking set. Despite only using the C_{α} atoms from the protein, PostNetDiMa obtained the same success rate to identify a native-like pose at top-1 position and even slightly outperformed flexible docking using Smina when considering the top-5 poses (Figure 12). Interestingly for almost all systems a top-5 ranked pose was identified within an RMSD of less than 4 Å. This means that the general

orientation of the scaffold of a ligand could be identified for almost all systems based on a coarse grained representation of the protein.

Furthermore Figure 13 highlights a strong correlation between prediction quality of the protein-ligand distance matrix and the docking quality. In particular, a native-like pose could most likely be generated among the top-5 ranked poses if the correlation coefficient r^2 between experimental and predicted distance matrix is larger than 0.8, and such a native-like pose is top ranked if r^2 is even larger than 0.9. Thus, in the future we will focus on improving the model for predicting the protein-ligand distance matrix, as this will directly improve docking performance beyond the quality of full-atomistic flexible docking programs.

Conclusion

We demonstrated in this study how flexible docking performance can be significantly improved using deep learning approaches. Two different models have been designed for this task: RerankGAT, a model based on graph convolutional neural networks, which was used to rerank existing poses. Besides standard docking algorithms, those poses could also be obtained from molecular dynamics simulations or similarity-based alignment algorithms. The second model, PoseNetDiMa, that generates distance matrices between ligands and proteins based on ligand topology and C_α atoms of binding site residues, can also be used for reranking poses. Furthermore, PoseNetDiMa also provides the necessary information to directly guide ligand placement.

Analysis of targets used in flexible docking reveals that standard docking strategies show weak accuracy in binding pose generation for flexible proteins and proteins with large binding sites compared to ligand size. Using distance matrices that are based on C_α atoms only, explicit side-chain sampling becomes obsolete, reducing the degrees-of-freedom significantly. This can result in more efficient and accurate sampling of native-like poses.

References

- (1) Murray, C. W.; Baxter, C. A.; Frenkel, A. D. The sensitivity of the results of molecular docking to induced fit effects: application to thrombin, thermolysin and neuraminidase. *Journal of computer-aided molecular design* **1999**, *13*, 547–562.
- (2) Englebienne, P.; Moitessier, N. Docking ligands into flexible and solvated macromolecules. 4. Are popular scoring functions accurate for this class of proteins? *Journal of chemical information and modeling* **2009**, *49*, 1568–1580.
- (3) Lill, M. A. Efficient Incorporation of Protein Flexibility and Dynamics into Molecular Docking Simulations. *Biochemistry* **2011**, *50*, 6157–6169.
- (4) Totrov, M.; Abagyan, R. Flexible ligand docking to multiple receptor conformations: a practical alternative. *Current opinion in structural biology* **2008**, *18*, 178–184.
- (5) Durrant, J. D.; McCammon, J. A. Computer-aided drug-discovery techniques that account for receptor flexibility. *Current opinion in pharmacology* **2010**, *10*, 770–774.
- (6) Henzler, A. M.; Rarey, M. In Pursuit of Fully Flexible Protein-Ligand Docking: Modeling the Bilateral Mechanism of Binding. *Molecular Informatics* **2010**, *29*, 164–173.
- (7) A Sotriffer, C. Accounting for induced-fit effects in docking: what is possible and what is not? *Current topics in medicinal chemistry* **2011**, *11*, 179–191.
- (8) Ferrari, A. M.; Wei, B. Q.; Costantino, L.; Shoichet, B. K. Soft docking and multiple receptor conformations in virtual screening. *Journal of medicinal chemistry* **2004**, *47*, 5076–5084.
- (9) Sherman, W.; Day, T.; Jacobson, M. P.; Friesner, R. A.; Farid, R. Novel procedure for modeling ligand/receptor induced fit effects. *Journal of medicinal chemistry* **2006**, *49*, 534–553.

- (10) Mahmoud, A. H.; Masters, M. R.; Yang, Y.; Lill, M. A. Elucidating the multiple roles of hydration for accurate protein-ligand binding prediction via deep learning. *Communications Chemistry* **2020**, *3*, 1–13.
- (11) Ghanbarpour, A.; Mahmoud, A. H.; Lill, M. A. On-the-fly Prediction of Protein Hydration Densities and Free Energies using Deep Learning. *arXiv preprint arXiv:2001.02201* **2020**,
- (12) Masters, M. R.; Mahmoud, A. H.; Yang, Y.; Lill, M. A. Efficient and Accurate Hydration Site Profiling for Enclosed Binding Sites. *Journal of chemical information and modeling* **2018**, *58*, 2183–2188, PMID: 30289252.
- (13) Senior, A. W.; Evans, R.; Jumper, J.; Kirkpatrick, J.; Sifre, L.; Green, T.; Qin, C.; Žídek, A.; Nelson, A. W.; Bridgland, A., et al. Improved protein structure prediction using potentials from deep learning. *Nature* **2020**, *577*, 706–710.
- (14) Senior, A. W.; Evans, R.; Jumper, J.; Kirkpatrick, J.; Sifre, L.; Green, T.; Qin, C.; Žídek, A.; Nelson, A. W.; Bridgland, A., et al. Protein structure prediction using multiple deep neural networks in the 13th Critical Assessment of Protein Structure Prediction (CASP13). *Proteins: Structure, Function, and Bioinformatics* **2019**, *87*, 1141–1148.
- (15) Hoffmann, M.; Noé, F. Generating valid Euclidean distance matrices. *arXiv preprint arXiv:1910.03131* **2019**,
- (16) Lim, J.; Ryu, S.; Park, K.; Choe, Y. J.; Ham, J.; Kim, W. Y. Predicting Drug–Target Interaction Using a Novel Graph Neural Network with 3D Structure-Embedded Graph Representation. *Journal of chemical information and modeling* **2019**, *59*, 3981–3988.
- (17) Ryu, S.; Lim, J.; Hong, S. H.; Kim, W. Y. Deeply learning molecular structure-property relationships using attention-and gate-augmented graph convolutional network. *arXiv preprint arXiv:1805.10988* **2018**,

- (18) Sun, M.; Zhao, S.; Gilvary, C.; Elemento, O.; Zhou, J.; Wang, F. Graph convolutional networks for computational drug development and discovery. *Briefings in bioinformatics* **2019**,
- (19) Morris, C.; Ritzert, M.; Fey, M.; Hamilton, W. L.; Lenssen, J. E.; Rattan, G.; Grohe, M. Weisfeiler and leman go neural: Higher-order graph neural networks. Proceedings of the AAAI Conference on Artificial Intelligence. 2019; pp 4602–4609.
- (20) Lei, T.; Jin, W.; Barzilay, R.; Jaakkola, T. Deriving neural architectures from sequence and graph kernels. Proceedings of the 34th International Conference on Machine Learning-Volume 70. 2017; pp 2024–2033.
- (21) Jin, W.; Coley, C.; Barzilay, R.; Jaakkola, T. Predicting organic reaction outcomes with weisfeiler-lehman network. Advances in Neural Information Processing Systems. 2017; pp 2607–2616.
- (22) Coley, C. W.; Jin, W.; Rogers, L.; Jamison, T. F.; Jaakkola, T. S.; Green, W. H.; Barzilay, R.; Jensen, K. F. A graph-convolutional neural network model for the prediction of chemical reactivity. *Chemical science* **2019**, *10*, 370–377.
- (23) Wang, X.; Ji, H.; Shi, C.; Wang, B.; Ye, Y.; Cui, P.; Yu, P. S. Heterogeneous graph attention network. The World Wide Web Conference. 2019; pp 2022–2032.
- (24) Koes, D. R.; Baumgartner, M. P.; Camacho, C. J. Lessons learned in empirical scoring with smina from the CSAR 2011 benchmarking exercise. *Journal of chemical information and modeling* **2013**, *53*, 1893–1904.
- (25) Wierbowski, S. D.; Wingert, B. M.; Zheng, J.; Camacho, C. J. Cross-docking benchmark for automated pose and ranking prediction of ligand binding. *Protein Science* **2020**, *29*, 298–305.

- (26) Hu, J.; Liu, Z.; Yu, D.-J.; Zhang, Y. LS-align: an atom-level, flexible ligand structural alignment algorithm for high-throughput virtual screening. *Bioinformatics* **2018**, *34*, 2209–2218.
- (27) Majewski, M.; Carmona, S. R.; Barril, X. Are protein-ligand complexes robust structures? *bioRxiv* **2019**, 454165.

List of Figures

- 1 Two neural network approaches to improve flexible docking performance. A. Gated attention neural network (RerankGAT) re-ranks poses obtained from standard docking program, here Smina, aiming to improve pose scoring. B. Graph neural network that predicts distance matrix between ligand atoms and protein C_α atoms (PoseNetDiMa) using protein C_α atom coordinates and ligand topology as input. The predicted distance matrix can be directly used to generate poses with implicit inclusion of side chain flexibility. 24
- 2 Two different types of graphs are encoded using graph neural network (GNN). One graph used the C_α atoms of the binding site residues as nodes colored by type of amino acid. Edges are colored based on distance between connecting C_α atoms. The second graph encodes the ligand topology using all heavy atoms. The atom nodes are colored by atom properties, the edges by bond character. 25
- 3 A. Scheme of a graph convolution step (*left*) and its attention-augmented version (*right*). Central nodes update is carried out using neighboring nodes where different width of arrows reflect the importance of information transfer, hence attention. B. Different versions of skip connections to conserve initial node features over multiple update steps. Skip rate z_v is determined using neural network layer. 26
- 4 Scheme of PoseNetDiMa to predict distance matrix based on coarse grained representation of protein and 2D representation of ligand. After initial local encoding using message pass (A), a local feature vector is determined based on combining atom encoding and bond featurization for protein and ligand separately (B). Using global attention (C) protein and ligand encodings are combined and a final global feature vector is computed (D). Local and global feature vector are finally combined to predict the protein-ligand distance matrix (E). 27
- 5 Scheme for using PoseNetDiMa for docking. A. Distance matrix is predicted using PostNetDiMa. B. For every ligand atom, all possible locations are computed based on the predicted distance matrix using all possible protein triplets. C. Those points are clustered using QT clustering algorithm. D. A maximum of 25 pharmacophore models are generated by random selection of combinations of cluster centers. Docking is performed to pharmacophore models using LSAlign. E. Those poses are rescored using iDock and atomic density maps obtained from predicted distance matrix. 28
- 6 Ranking performance using Smina and rerankGAT (top) on all systems and (bottom) on systems with at least one native-like pose. 29
- 7 (Top) Fraction of systems with certain distance matrix prediction accuracy measured by correlation coefficient between experimental and predicted distance matrix. (Bottom) Fraction of systems with native-like pose using Smina correlated with the distance matrix prediction accuracy. 30
- 8 Ranking performance using Smina and rerankGAT (top) on all systems and (bottom) on systems with at least one native-like pose for cross-docking data set. 31

9	(Top) Fraction of systems with certain distance matrix prediction accuracy measured by correlation coefficient between experimental and predicted distance matrix. (Bottom) Fraction of systems with native-like pose using Smina correlated with the distance matrix prediction accuracy. Data for cross-docking data set is shown.	32
10	Scheme for pose re-ranking using poseNetDiMa. Protein-ligand distance matrix is predicted using postNetDiMa and compared with corresponding distance matrices measured for each docking pose. Re-ranking is performed based on similarity between predicted distance matrix and distance matrix of a given docking pose.	33
11	Re-ranking accuracy of docking poses obtained from Smina using PoseNetDiMa for systems with native-like poses using only docked poses (left) or when adding native poses from X-ray structure (right).	34
12	Cumulative probability of predicting docking pose within certain RMSD to native binding mode at top-1 or among top-5 ranked solutions using PostNetDiMa in docking modus.	35
13	Probability of predicting native-like docking poses within an RMSD of less than 2 Å (blue) and 4 Å (orange) to the native binding mode at top-1 or among top-5 ranked solutions using PostNetDiMa in docking modus. Dependency on prediction quality of distance matrix is shown.	36

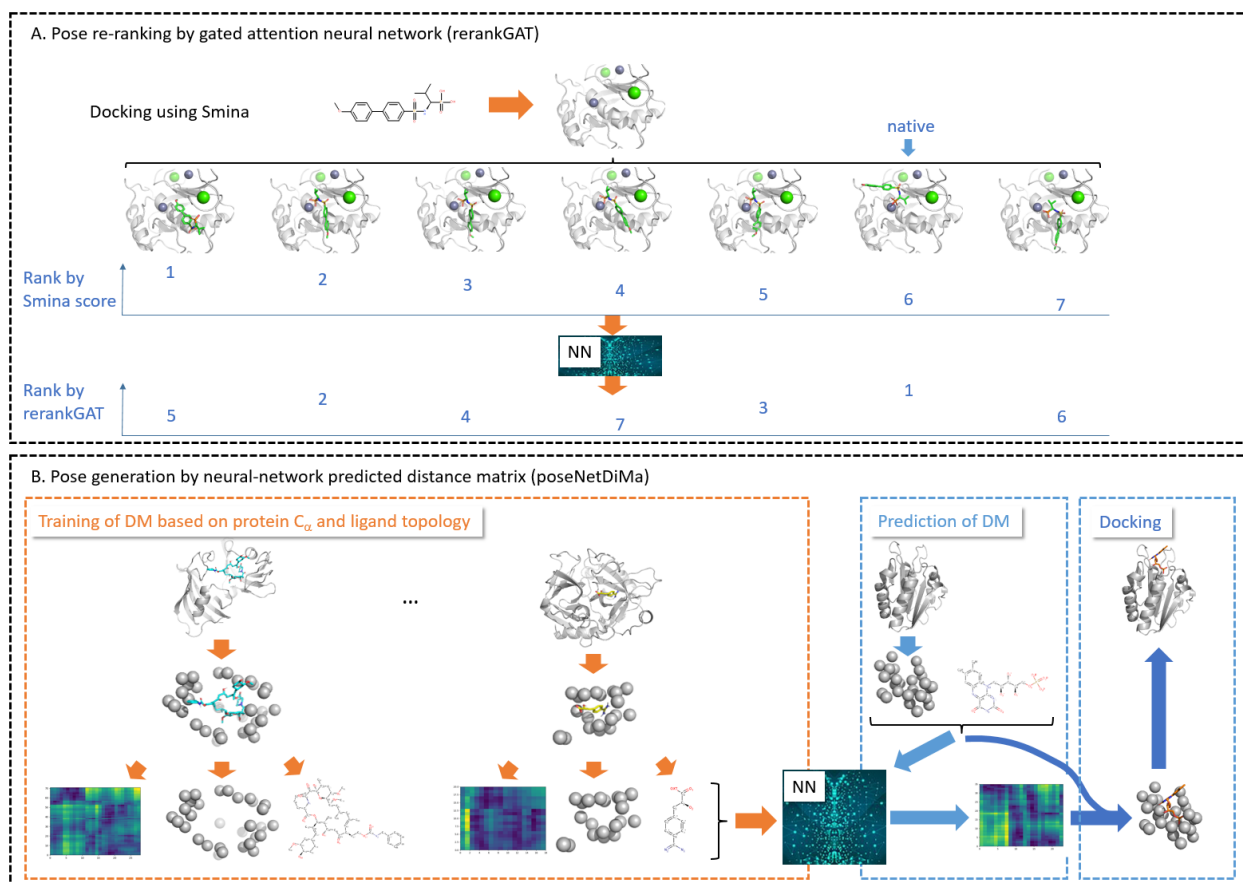


Figure 1: Two neural network approaches to improve flexible docking performance. A. Gated attention neural network (RerankGAT) re-ranks poses obtained from standard docking program, here Smina, aiming to improve pose scoring. B. Graph neural network that predicts distance matrix between ligand atoms and protein C_α atoms (PoseNetDiMa) using protein C_α atom coordinates and ligand topology as input. The predicted distance matrix can be directly used to generate poses with implicit inclusion of side chain flexibility.

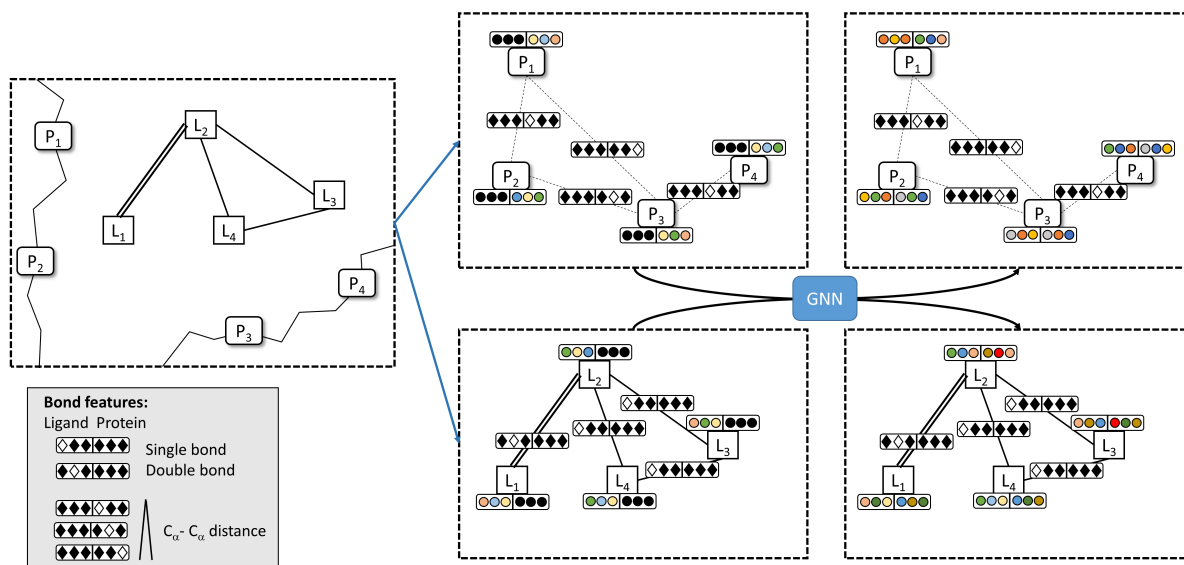


Figure 2: Two different types of graphs are encoded using graph neural network (GNN). One graph used the C_{α} atoms of the binding site residues as nodes colored by type of amino acid. Edges are colored based on distance between connecting C_{α} atoms. The second graph encodes the ligand topology using all heavy atoms. The atom nodes are colored by atom properties, the edges by bond character.

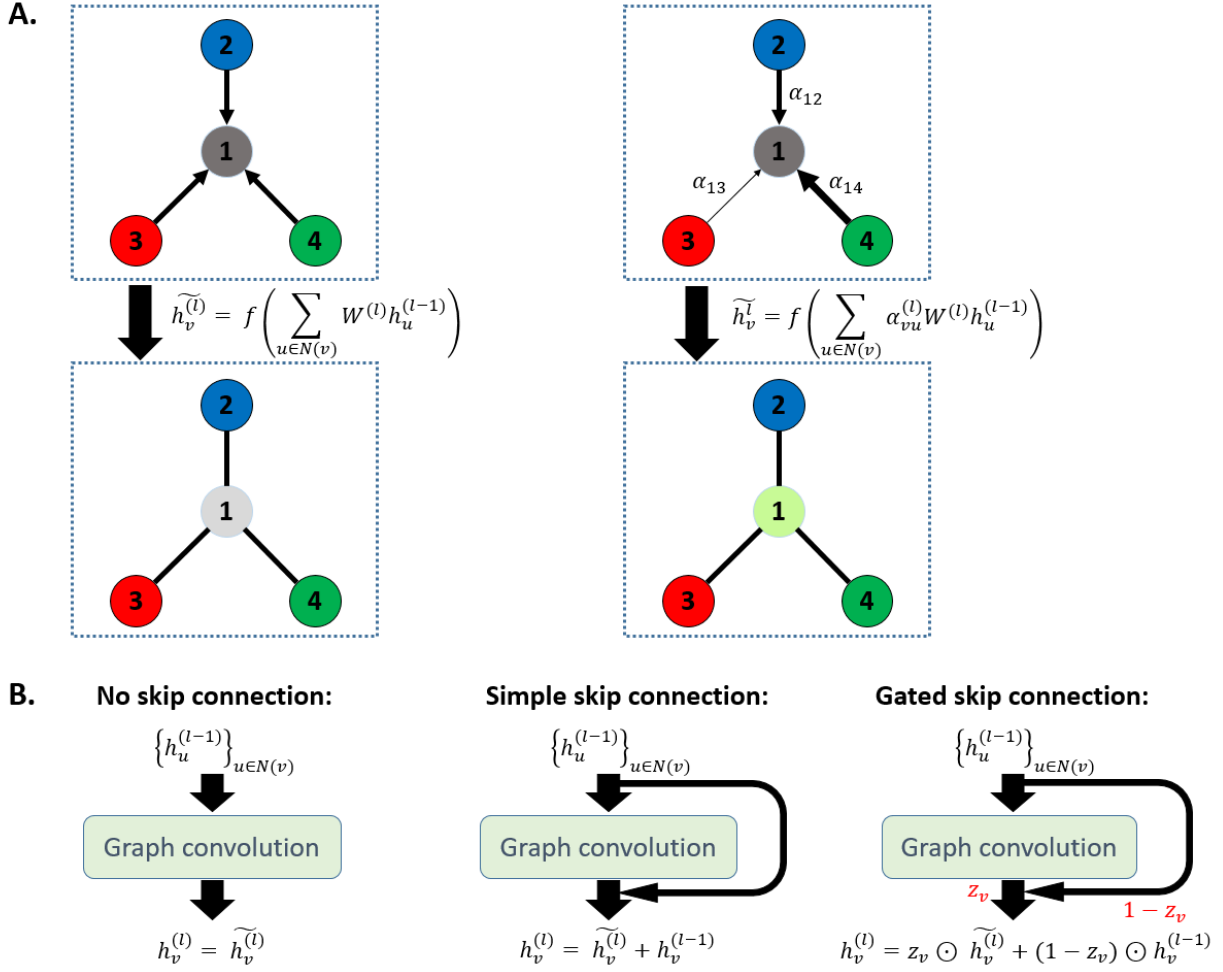


Figure 3: A. Scheme of a graph convolution step (*left*) and its attention-augmented version (*right*). Central nodes update is carried out using neighboring nodes where different width of arrows reflect the importance of information transfer, hence attention. B. Different versions of skip connections to conserve initial node features over multiple update steps. Skip rate z_v is determined using neural network layer.

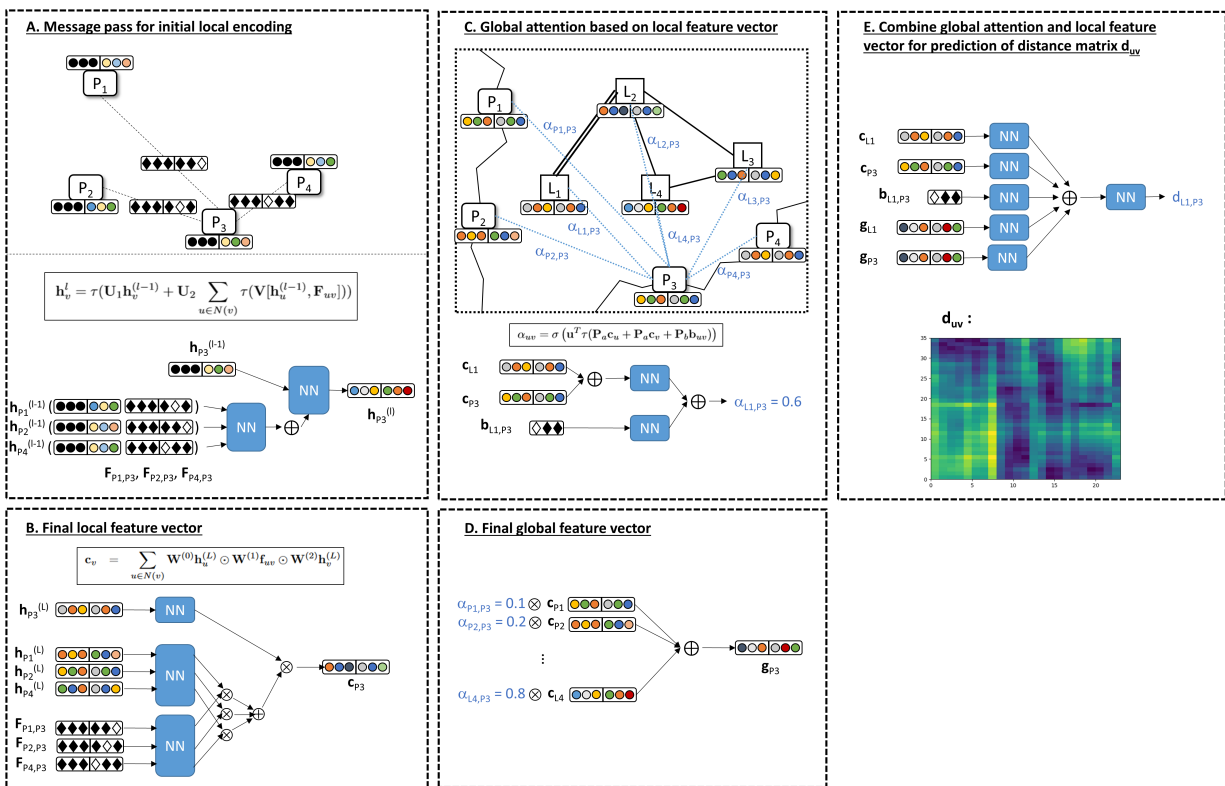


Figure 4: Scheme of PoseNetDiMa to predict distance matrix based on coarse grained representation of protein and 2D representation of ligand. After initial local encoding using message pass (A), a local feature vector is determined based on combining atom encoding and bond featurization for protein and ligand separately (B). Using global attention (C) protein and ligand encodings are combined and a final global feature vector is computed (D). Local and global feature vector are finally combined to predict the protein-ligand distance matrix (E).

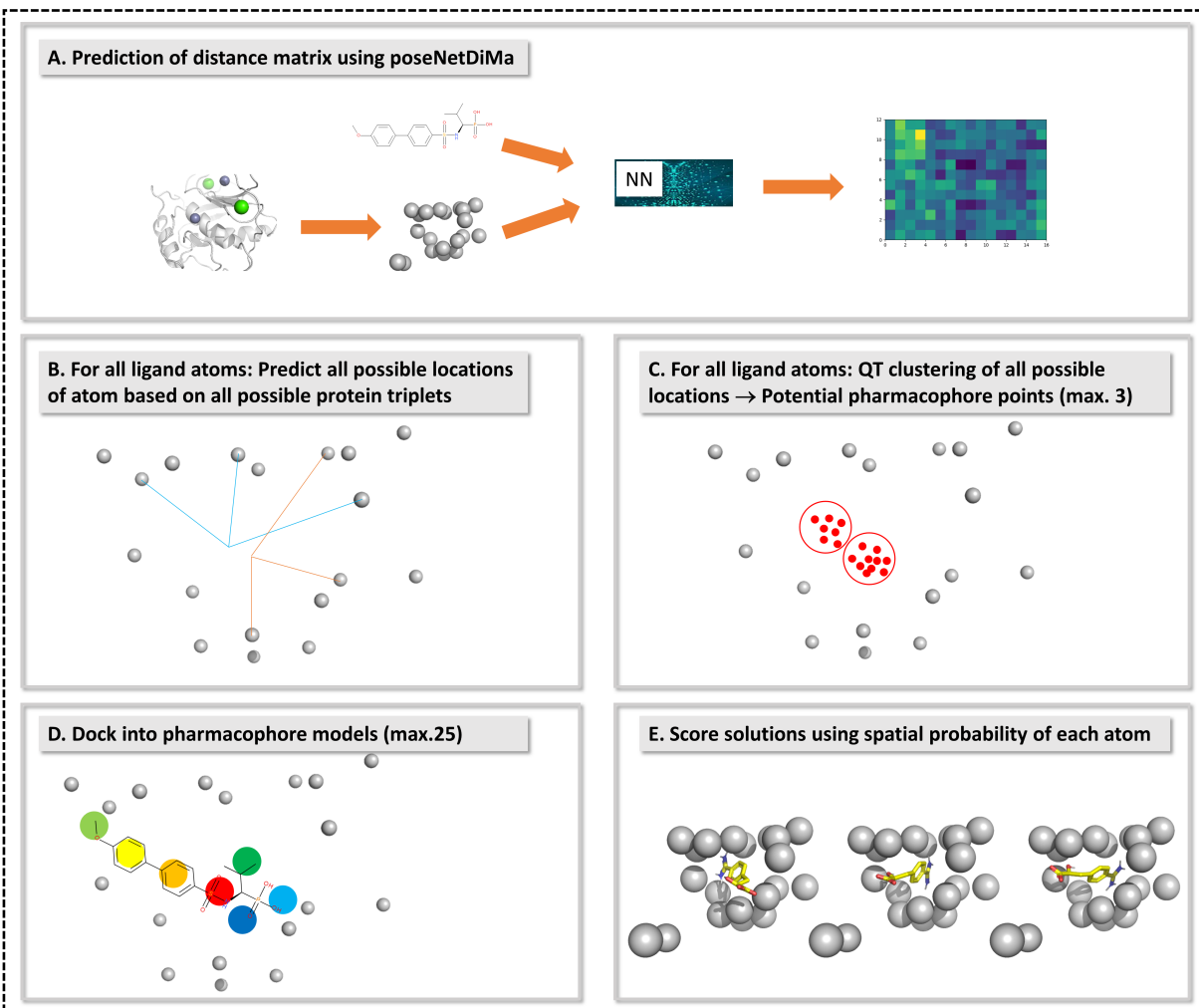


Figure 5: Scheme for using PoseNetDiMa for docking. A. Distance matrix is predicted using PostNetDiMa. B. For every ligand atom, all possible locations are computed based on the predicted distance matrix using all possible protein triplets. C. Those points are clustered using QT clustering algorithm. D. A maximum of 25 pharmacophore models are generated by random selection of combinations of cluster centers. Docking is performed to pharmacophore models using LSAAlign. E. Those poses are rescored using iDock and atomic density maps obtained from predicted distance matrix.

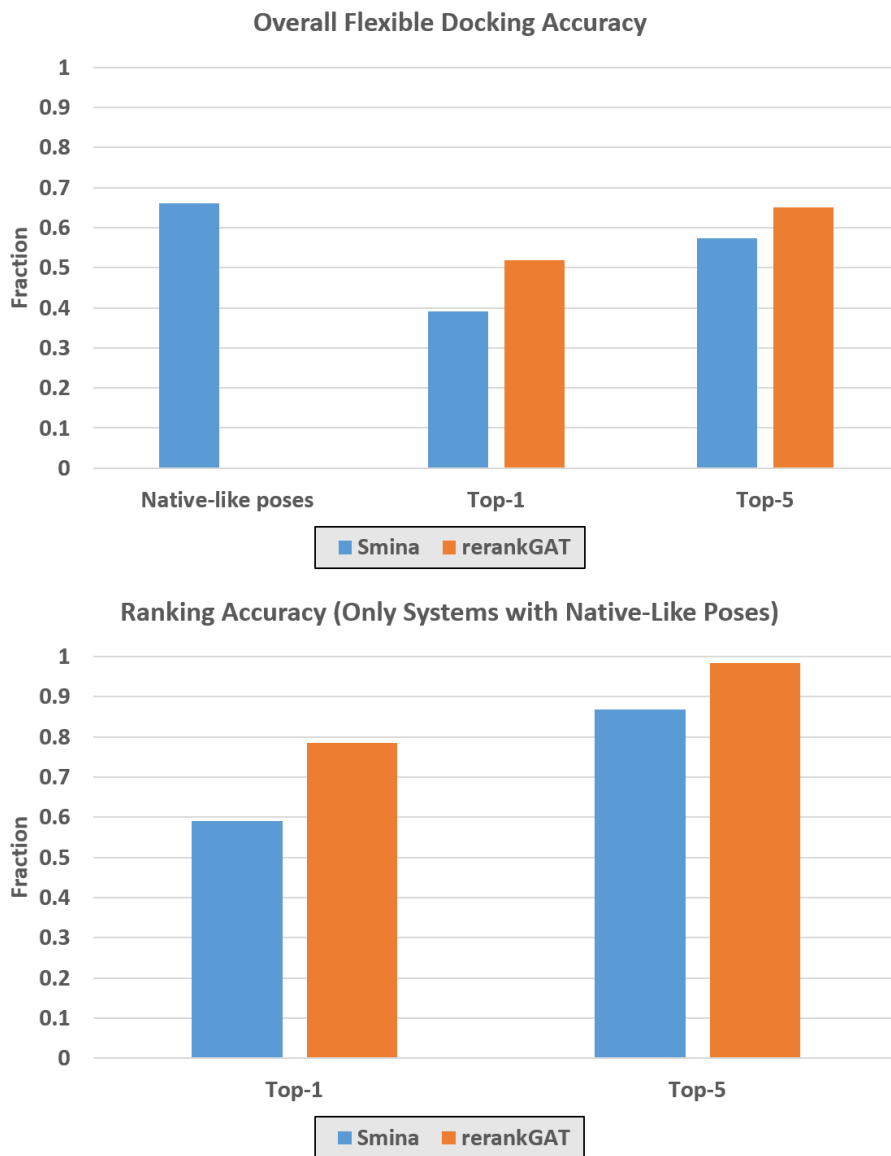


Figure 6: Ranking performance using Smina and rerankGAT (top) on all systems and (bottom) on systems with at least one native-like pose.

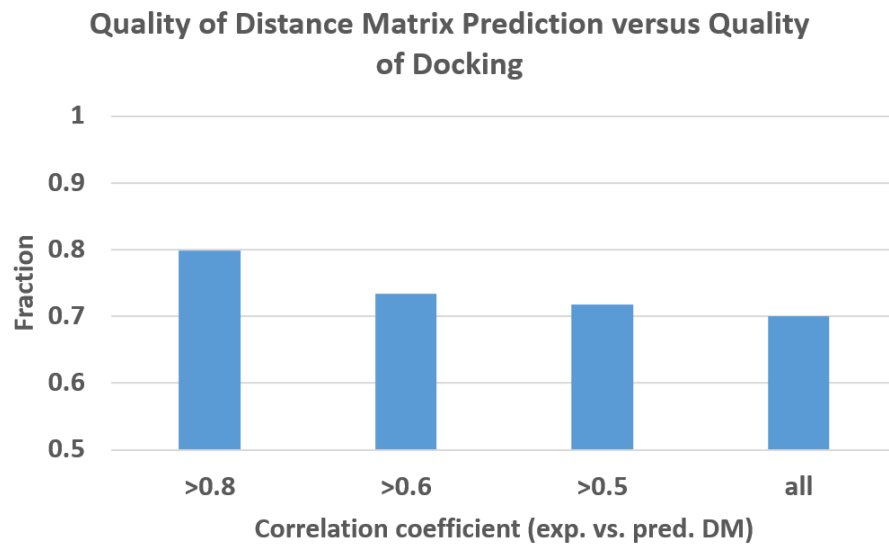
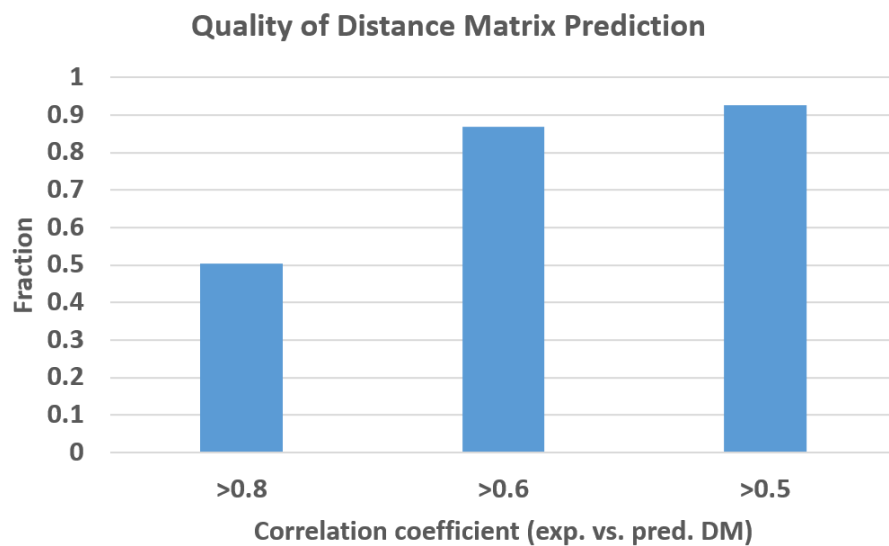


Figure 7: (Top) Fraction of systems with certain distance matrix prediction accuracy measured by correlation coefficient between experimental and predicted distance matrix. (Bottom) Fraction of systems with native-like pose using Smina correlated with the distance matrix prediction accuracy.

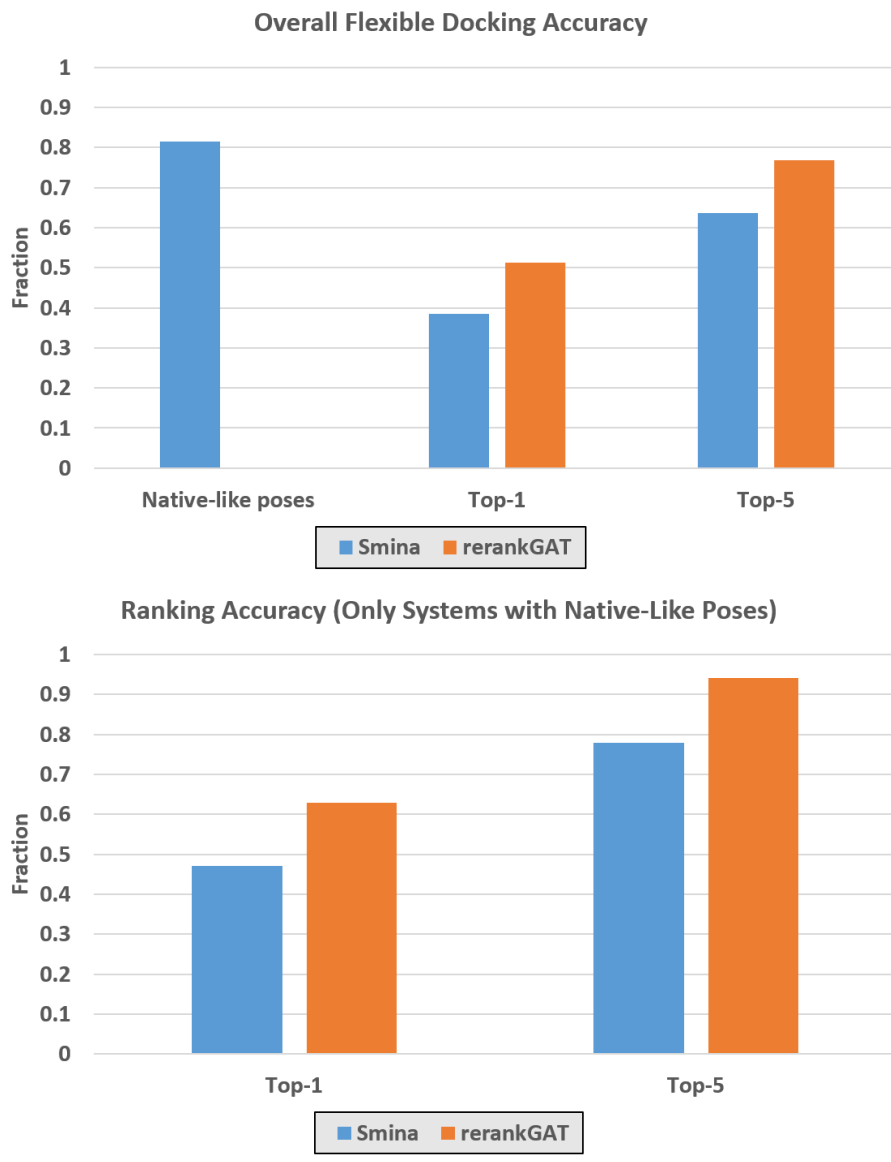


Figure 8: Ranking performance using Smina and rerankGAT (top) on all systems and (bottom) on systems with at least one native-like pose for cross-docking data set.

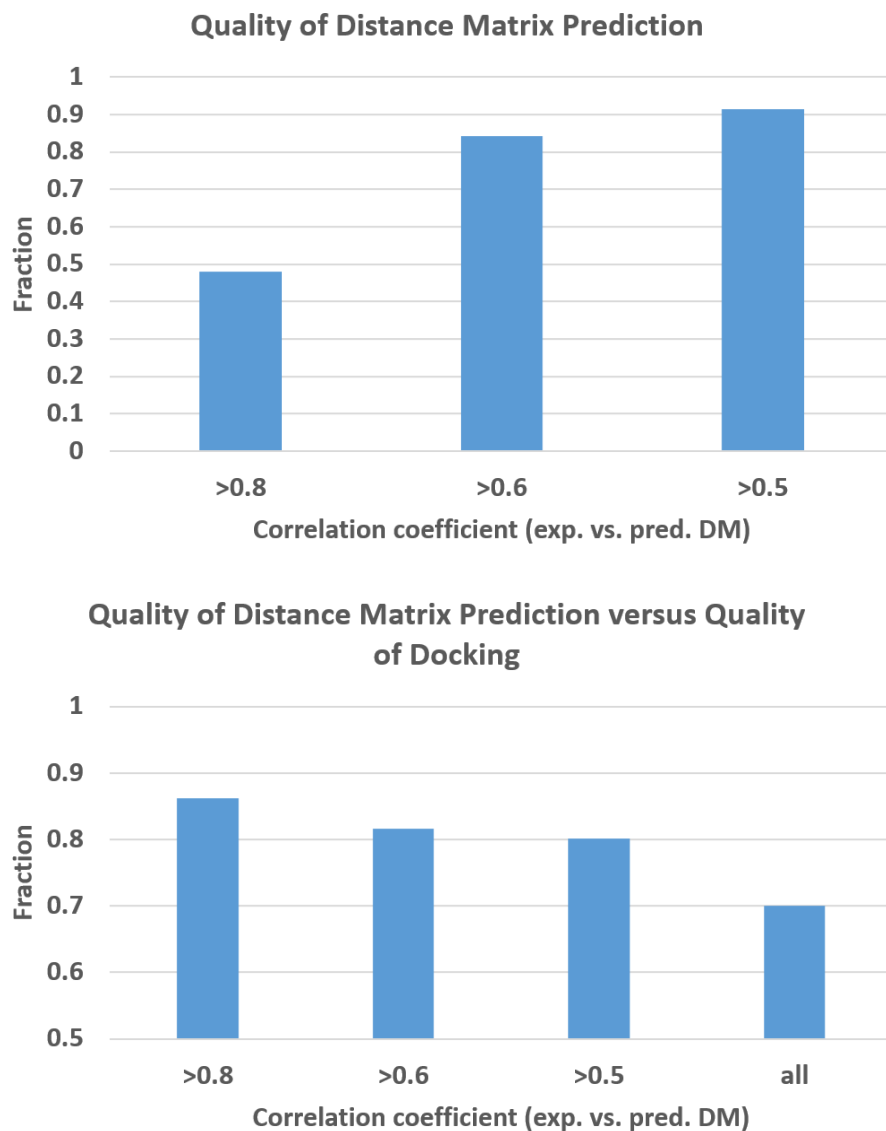


Figure 9: (Top) Fraction of systems with certain distance matrix prediction accuracy measured by correlation coefficient between experimental and predicted distance matrix. (Bottom) Fraction of systems with native-like pose using Smina correlated with the distance matrix prediction accuracy. Data for cross-docking data set is shown.

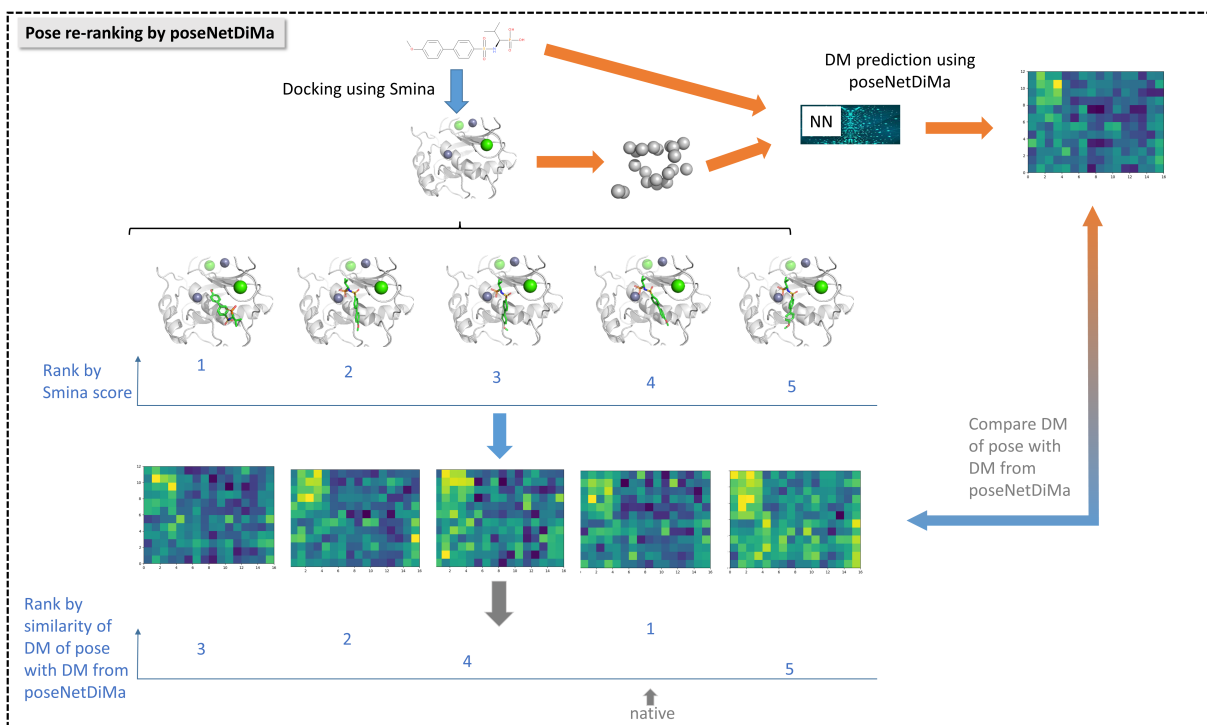


Figure 10: Scheme for pose re-ranking using poseNetDiMa. Protein-ligand distance matrix is predicted using postNetDiMa and compared with corresponding distance matrices measured for each docking pose. Re-ranking is performed based on similarity between predicted distance matrix and distance matrix of a given docking pose.

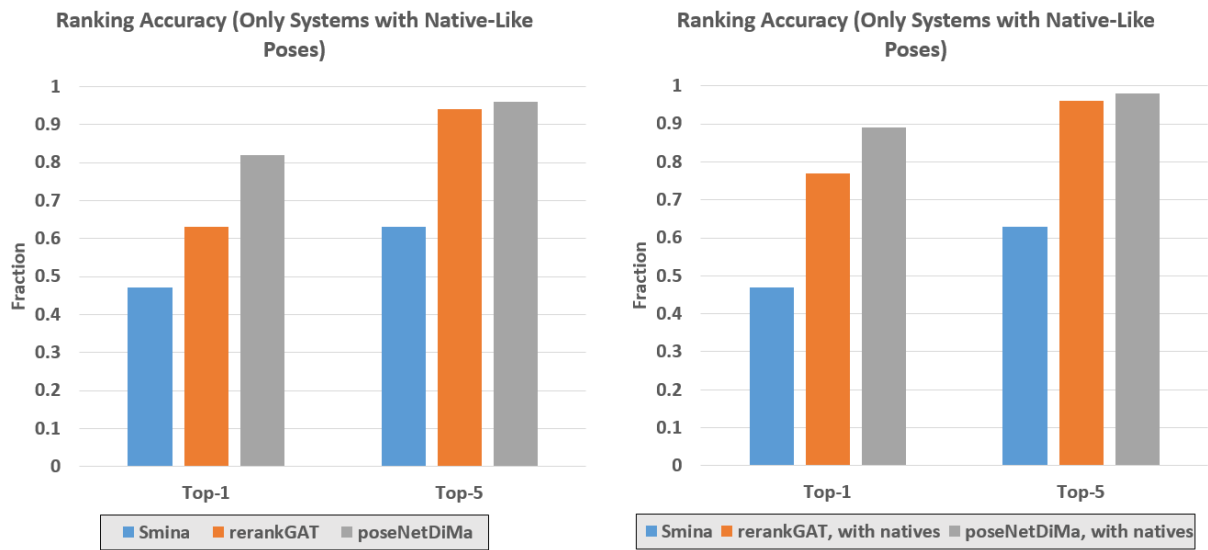


Figure 11: Re-ranking accuracy of docking poses obtained from Smina using PoseNetDiMa for systems with native-like poses using only docked poses (left) or when adding native poses from X-ray structure (right).

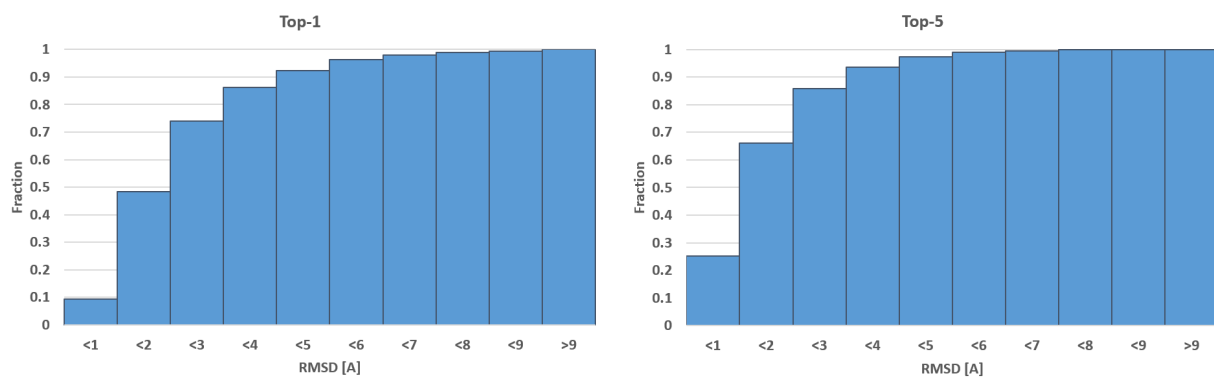


Figure 12: Cumulative probability of predicting docking pose within certain RMSD to native binding mode at top-1 or among top-5 ranked solutions using PostNetDiMa in docking modus.

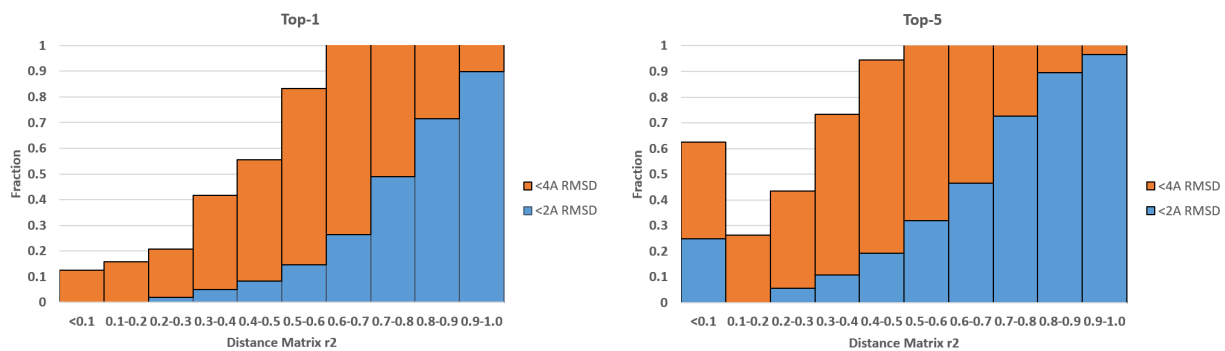


Figure 13: Probability of predicting native-like docking poses within an RMSD of less than 2 Å (blue) and 4 Å (orange) to the native binding mode at top-1 or among top-5 ranked solutions using PostNetDiMa in docking modus. Dependency on prediction quality of distance matrix is shown.